MANUSCRIPT ID NUMBER: JLT-38985-2025

Polarization- and Temperature-Insensitive 8x400GHz O-Band Cascaded AWG for Large Radix Data Center and AI/ML Networks

Robert Palmer, Henk Bulthuis, Cleitus Antony, *Member, IEEE*, Jakub Zvěřina, Gunter Beelen, Jad Sarkis, AbuBakar Bhatti, Giuseppe Talli, *Member, IEEE*, Maxim Kuschnerov, *Member, IEEE*

***Abstract*—We demonstrate a PLC-based O-Band 8-channel cascaded AWG design. The manufactured prototypes achieve 400 GHz channel spacing while simultaneously reaching a 1 dB bandwidth of 300 GHz and a crosstalk below -40 dB. The measured fiber-to-fiber loss is as low as 2.7 dB and the PDL is below 0.2 dB. We determine a low thermal drift of -1.8 GHz/Kelvin. The combination of low IL, high bandwidth, low crosstalk, and low thermal drift make the device particularly attractive for WDM-based data center and AI networks architectures that benefit from a large network switch radix.**

***Index Terms*—AWG, Demultiplexing, Integrated Optics, Multiplexing, PLC.**

I. INTRODUCTION

HIGH-radix, high-capacity electrical switches in spine-leaf network topologies are the heart of modern data centers and high-performance compute clusters [1]. The capacity of spine switches is doubling every two years. This is achieved by a doubling of the lane data rate and by an interleaved doubling of the number of channels every four years, e. g. Broadcom released the market's first 51.2 Tbps Tomahawk 5 switch with 512 lanes at 112 Gbps in 2023 [2] and the first 102.4 Tbps Tomahawk 6 switch with 512 lanes at 224 Gbps two years later in 2025 [3]. Hence, first 204.8 Tbps switches are expected in 2027, running at 224 Gbps per lane at 112 GBd PAM4 [4] with a total of 1024 lanes per switch. The combination of fast SERDES rates and large channel counts fueled the development of co-packaged optics transceivers [5], [6] targeting shoreline densities exceeding 1 Tbps/mm [7]. Such high shoreline densities not only require ultra-compact transmitters and receivers, but also space-efficient fiber-array interconnects. A standard fiber array unit (FAU) with 127 µm pitch, may support 1 polarization maintaining (PM) fiber for the external light source (ELS) input and 3 transmitter (TX) and receiver (RX) fiber pairs per mm, requiring more than 0.33 Tbps/fiber pair for meeting the >1 Tbps/mm target, which exceeds the 200 Gbps lane rate of next generation SERDES. To improve the shoreline density of the fiber interconnect, two strategies have been reported: 1) reduced cladding fibers [8] or PLC pitch converters [9] are used to reduce the optical I/O pitch of the CPO device or 2) the fiber capacity is increased through WDM [7], [10]. While the reduction of the fiber pitch may improve the I/O density by a factor of 2-3, the use of WDM has the potential to increase the density by a factor of 10 or beyond. Such WDM approaches, however, go along with a more complex transceiver architecture, calling for passive or active integrated multiplexers (MUX) and demultiplexers (DEMUX) [11], [12]. However, this high capacity per fiber may be impractical for achieving high-radix switches and thus flat networks [1], which can lower the power consumption and latency [13] of node-to-node interconnects. For enabling such networks, optical (de-)multiplexers may be used to break out the high-capacity WDM into individual 200G channels. Such optical (de-)multiplexers may be realized as arrayed waveguide gratings (AWG), Echelle gratings [14] or as a concatenation of unbalanced Mach-Zehnder-Interferometers (MZI) [15] and require low loss, low crosstalk, low polarization dependency and low thermal drift. The selected wavelengths are typically in the O-band to minimize dispersion related transmission penalties [16]. The ideal WDM grid for such applications is usually a compromise between achievable flattop response of the filter and its residual temperature dependency. While a 200 GHz grid would offer the highest potential in scaling the number of 224 Gbps channels, it provides close to no margin for thermal drift and manufacturing tolerances for optical (de-)multiplexers. We will show that even a low temperature dependent material like SiO_2 calls for a relaxed frequency grid requirement of ~400 GHz, for passive (de-)multiplexing.

This paragraph of the first footnote will contain the date on which you submitted your paper for review, which is populated by IEEE. We acknowledge funding by the EU HORIZON 2021 project ADOPTION (grant agreement 101070178). (Corresponding author: Robert Palmer)

Robert Palmer, Jad Sarkis, Giuseppe Talli, and Maxim Kuschnerov are with Huawei Heisenberg Research Center (Munich), Riesstr. 25, 80992 Munich, Germany (e-mails: robert.palmer@huawei.com, jad.sarkis@huawei.com, giuseppe.talli@huawei.com, maxim.kuschnerov@huawei.com).

Henk Bulthuis and Gunter Beelen are with Broadex Technologies UK Ltd., Starlaw Park, Starlaw Road, Livingston EH54 8SF, United Kingdom (emails: henk.bulthuis@broadex-tech.co.uk, gunter.beelen@broadex-tech.co.uk).

Jakub Zvěřina is with Argotech, Náchodská 529, 541 01 Trutnov, Czech Republic (e-mail: jakub.zvěřina@argotech.cz).

Cleitus Antony is with Tyndall National Institute, School of Physics, University College Cork, Lee Maltings, Dyke Parade, Cork, Ireland. T12 R5CP (e-mail: cleitus.antony@tyndall.ie).

AbuBakar Bhatti is with SENKO Advanced Components (Euro) Ltd., Unit 2, Rankine Road, Basingstoke, RG24 8PP, United Kingdom (e-mail: AbuBakar.Bhatti@senko.com).

Color versions of one or more of the figures in this article are available online at http://ieeexplore.ieee.org

This article has been accepted for publication in Journal of Lightwave Technology. This is the author's version which has not been fully edited and content may change prior to final publication. Citation information: DOI 10.1109/JLT.2026.3660127

It has long been the goal of the optics industry to provide low loss box-shape filter products using volume manufacturing techniques. Planar lightwave circuits (PLC) based on silica-on-silicon technology have become a leading platform for realizing compact and reliable AWG multiplexers. A comprehensive overview of silica planar lightwave circuits has been published by C.R. Doerr and K. Okamoto [17]. The PLC platform offers several advantages, including low insertion loss (IL), low polarization dependent loss (PDL), low thermal drift, and efficient coupling to standard fiber optics.

Temperature-insensitive operation is a key device property when targeting passive demultiplexers. The temperature dependency of silica-based devices [18] is a factor ten lower as compared to its higher-index contrast counterparts based on e.g. InP [19] and Si [20] and even a factor two lower compared to Si_3N_4-based devices [21]. Furthermore, Si-, InP-, and Si_3N_4-based devices are usually strongly birefringent, requiring special engineering solutions for realizing AWGs with moderate to low polarization dependency, e.g. using polarization diversity [22], insertion of polarization rotators into the middle of the AWG [23], using thick core layers to lower birefringence [24], or by excitation of multiple inputs [25]. Despite these efforts, these devices lag behind silica-based AWGs [26] in terms of simultaneously meeting PDL, IL, crosstalk, and temperature insensitivity targets at high manufacturing yield.

In this paper, we present a comprehensive study of a flattop integrated cascaded AWG (CAWG) [27], [28] demultiplexer based on silica-on-silicon. We analyze the performance of the PLC-based CAWG and compare it to characteristics of conventional AWGs and cascade MZI-AWGs. The discussion focuses on key performance indicators such as insertion loss, bandwidth, crosstalk, polarization dependency and thermal drift, highlighting the unique advantages of the PLC platform for high-performance AWG applications. Compared to earlier work published on cascade AWG [29] we achieved a record low fiber-to-fiber loss of 2.7 dB. Furthermore, the CAWG was made with an etch technique that achieves improved isolation between the individual AWGs, resulting in superior crosstalk between the CAWG channels. The remainder of this paper is organized as follows: Section II defines the targeted application for the demonstrated DEMUX. From this, we derive the high-level specifications for the AWG in section III. The design of the cascaded AWG is illustrated in section IV. The fabricated devices and their performance are discussed in section V and we compare the key performance indicators of our DEMUX design with competing approaches in silica and other material platforms.

II. Targeted DEMUX application

The cascaded O-band AWG has been developed within EU HORIZON 2021 project ADOPTION (grant 101070178) [30], which is targeting innovative architectures and components for hyperscale data center, artificial intelligence (AI), machine learning (ML) and high-performance computing (HPC) applications, such as co-packaged optics (CPO) based transceivers [5], [6], [31] and fast optical switches [32]. As discussed in the Introduction, generally such CPO transceivers rely on single-wavelength transmission with high fiber counts, or utilize wavelength-division multiplexing to increase the capacity per fiber. Within ADOPTION, CPO transceivers are developed that multiplex 16 channels on a 200 GHz or 8 channels on a 400 GHz grid, driven at 112 GBd, see Fig. 1(a). While this results in a total capacity of 1.6 Tbps per fiber, when deployed as part of a co-packaged optics switch, the achievable switch radix is rather limited. E.g. for leaf switches a larger radix with direct 100G or 200G links can be advantageous. This can be realized by mating the ADOPTION CPO with a device that we refer to as an optical port breakout, which can be built as an unamplified or amplified AWG, see Fig. 1(b). The optical port breakout acts as a wavelength demultiplexing interface between the high-capacity WDM fiber of the CPO module and individual lower-rate client ports. In its passive form, it provides a purely spectral separation function, while an amplified variant can include an integrated semiconductor optical amplifier stage to compensate insertion loss for extended reach or fan-out applications. Such an AWG has stringent system requirements on insertion loss, bandwidth, and on the crosstalk between channels. Section III summarizes the requirements as high-level device specifications.

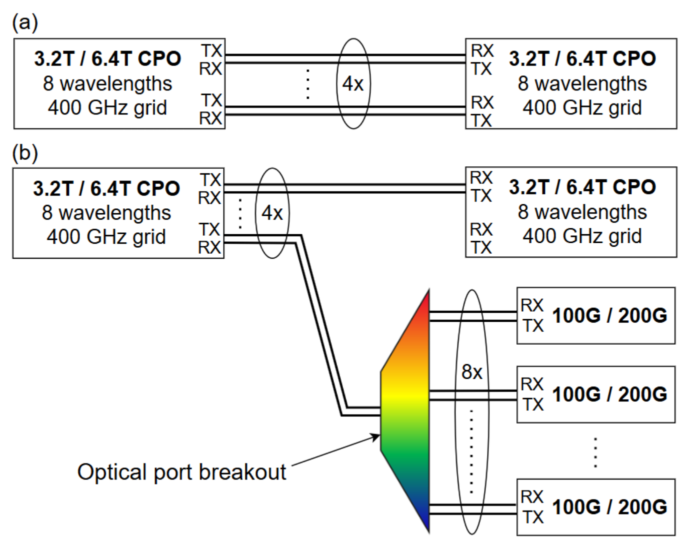

Fig. 1. DEMUX application example. (a) A CPO module transmits 112 GBd NRZ or PAM4 per wavelength on eight 400 GHz spaced wavelengths over four transmit fibers, yielding 3.2 Tbps / 6.4 Tbps (NRZ / PAM4) total capacity per direction. (b) The radix of the CPO can be expanded by separating the fiber pairs and spectrally demultiplexing the individual wavelengths using a low-loss, low-crosstalk “optical port breakout” device.

III. Device Specifications

The high-level specifications of the AWG are summarized in TABLE I and illustrated in Fig. 2. The targeted wavelength plan is aligned with the DWDM-MSA [33] and is depicted in

This article has been accepted for publication in Journal of Lightwave Technology. This is the author's version which has not been fully edited and content may change prior to final publication. Citation information: DOI 10.1109/JLT.2026.3660127

TABLE II. The AWG is designed to be mated with a CPO transceiver that can support link budgets of 8 dB. We reserve 4 dB of loss to account for up to 2 km of SMF28 and fiber connector losses. Consequently, an unamplified optical port breakout device may have fiber-to-fiber losses of up to 3.5 dB with a residual margin of 0.5 dB.

The 112 GBd signals can suffer from filter-related transmission penalties and from temperature-induced frequency misalignment between laser and AWG. TABLE III depicts the recommended and the acceptable temperature ranges for data centers according to ASHRAE TC 9.9 [34]. The recommended temperature range spans 9 °C, while the worst-case acceptable range in class A4 spans 40 °C. Assuming a thermo-optic coefficient of SiO_2 of 8.2×10^{-6}/K [18], and including the contribution from the path-length expansion, which contributes another 3.3×10^{-6}/K, this corresponds to a frequency drift of the AWG filter function of ±8 GHz (±4.5 °C) and ±36 GHz (±20 °C), respectively.

TABLE I
HIGH-LEVEL SPECIFICATION FOR THE AWG, ASSUMING NRZ OR PAM4 SIGNALS AT 112 GBAUD.

Parameter	Target (NRZ / PAM4)
Insertion loss	< 3.5 dB
1 dB bandwidth	> 220 GHz
Grid	400 GHz
Wavelength plan	See TABLE II
Crosstalk with neighboring channels (at +/-100GHz)	< -27.0 dB / < -38.4 dB
Integrated crosstalk	< -23.5 dB / < -31.0 dB

TABLE II
DWDM-MSA [33] COMPLIANT WAVELENGTH PLAN.

Channel	Center frequency	Center wavelength
1	231.4 THz	1295.56 nm
2	231.0 THz	1297.80 nm
3	230.6 THz	1300.05 nm
4	230.2 THz	1302.31 nm
5	229.8 THz	1304.58 nm
6	229.4 THz	1306.85 nm
7	229.0 THz	1309.14 nm
8	228.6 THz	1311.43 nm

TABLE III
ASHRAE TC 9.9 [34] RECOMMENDED TEMPERATURE RANGES FOR DATA CENTERS.

Equipment class	Recommended temperature range (°C)	Acceptable temperature range (°C)
A1	18 to 27	15 to 32
A2	18 to 27	10 to 35
A3	18 to 27	5 to 40
A4	18 to 27	5 to 45

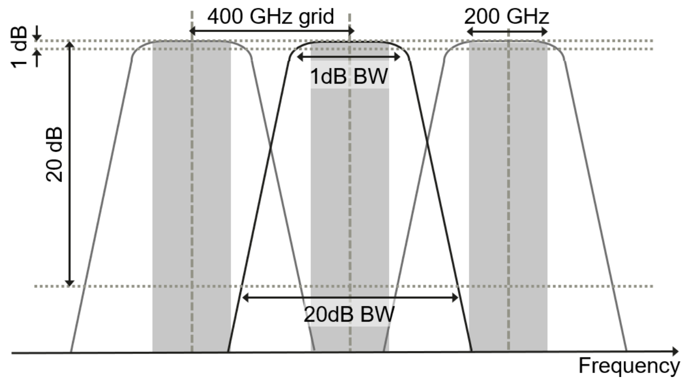

Fig. 2. Definition of filter specifications. The vertical dashed lines mark the location of the targeted frequencies. The gray 200 GHz wide areas mark the expected overlap with the input signals, composed of ~125 GHz signal bandwidth plus ~75 GHz for thermal drift.

Next, the bandwidth-related filter penalty is studied using VPItransmissionMaker™. The TX and RX bandwidth of the CPO lanes was set to 112 GHz and 56 GHz, respectively. We assume a CAWG passband shape as depicted in Fig. 12. The frequency axis is rescaled for achieving filters with varying 1 dB bandwidth, ranging from 100 GHz to 300 GHz. The receiver sensitivity penalty for 112 GBd NRZ and PAM4 as a function of the AWG's 1 dB bandwidth is depicted in Fig. 3(a). While ~150 GHz of bandwidth is sufficient to keep the penalty low (~0.1 dB for NRZ, ~0.7 dB for PAM4), no margin is given to allow for frequency offsets between the CPO output wavelength and the AWG channel. We target to support at least ±36 GHz frequency offset to cover the estimated thermal frequency drift within a 40 °C temperature span. This sets the lower bound for the 1 dB bandwidth to ~220 GHz. Increasing the bandwidth beyond this value is advantageous for relaxing frequency alignment requirements between CPO and AWG, as studied in Fig. 3(b). We find that a narrow 1 dB filter bandwidth of 130 GHz is very prone to misalignment and requires around 20 GHz of alignment accuracy. The targeted filter 1 dB bandwidth of 220 GHz relaxes the alignment requirement and gives sufficient margin for thermal drift: Up to ±62 GHz and ±70 GHz misalignment are allowed to keep the penalty below 0.5 dB in case of NRZ and PAM4, respectively. When increasing the filter's 1 dB bandwidth to 300 GHz, the misalignment tolerance increases to ~100 GHz.

The combination of AWG filter bandwidth, filter shape, and wavelength grid impacts the optical crosstalk between neighboring channels, see Fig. 2. Our definition of crosstalk refers to the residual transmitted power into the neighboring gray bands in Fig. 2, that mark the expected possible overlap of the filter with the input signals. In our use case, the width of such overlap span is set to 200 GHz and derives from the signal bandwidth of ~125 GHz plus ~75 GHz margin for thermal drift.

We analyze the crosstalk requirements of the DEMUX in the presence of 7 aggressor channels using an analytical receiver model [35] in Python. The channel under test is exposed to crosstalk from 2 neighboring channels and 5 non-neighboring channels. We assume a TX extinction ratio (ER) of 4 dB, 0.5 A/W input-referred RX photo diode responsivity, a TIA with input-referred noise density of 18 pA/√Hz, and a receiver bandwidth of 56 GHz. Each aggressor channel is treated as a white noise source that degrades the SNR of the received channel under test.

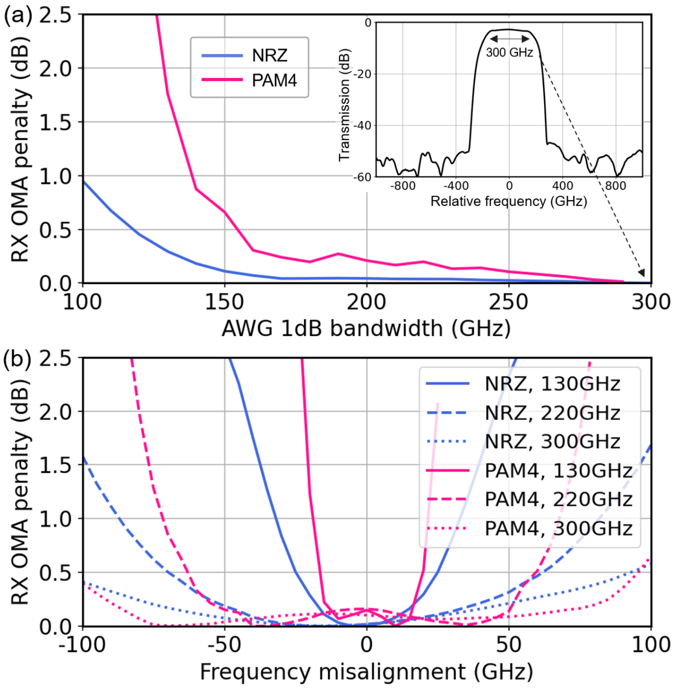

Fig. 3. Receiver sensitivity penalty for 112 GBd NRZ and PAM4 at a pre-FEC BER threshold of 1×10^{-3}. (a) Penalty as a function the 1 dB bandwidth of the demultiplexing AWG. At least 150 GHz of 1 dB bandwidth are required to limit the filter related penalty to 0.1 dB for NRZ and to 0.7 dB for PAM4. (b) Penalty as a function of frequency misalignment between signal and AWG passband center for filters with 1 dB bandwidth of 130 GHz, 220 GHz, and 300 GHz.

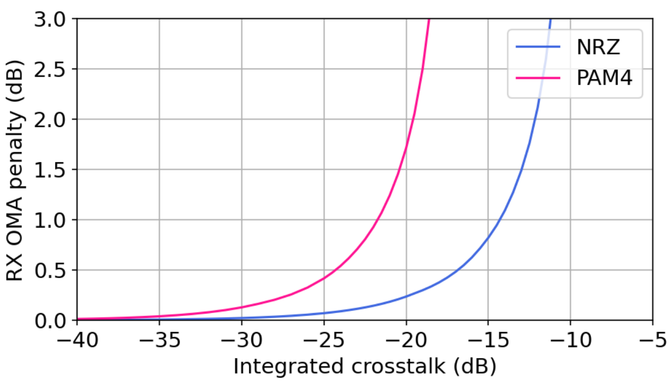

Fig. 4. Simulated sensitivity penalty of a 112 GBd NRZ and PAM4 signal at a pre-FEC BER threshold of 1×10^{-3} as a function of integrated crosstalk due to neighboring and non-neighboring channels.

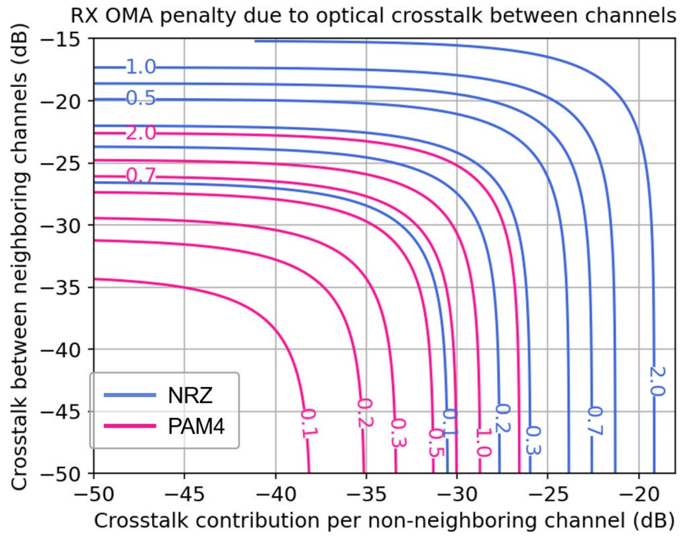

Fig. 5. Simulated sensitivity penalty in dB of an 8 channel 112 GBd NRZ (blue) or PAM4 (magenta) system as a function of crosstalk due to neighboring and non-neighboring channels at a pre-FEC BER threshold of 1×10^{-3}. Penalties above 2 dB are not depicted in the figure.

The simulated RX sensitivity penalty as a function of integrated crosstalk is depicted in Fig. 4 for 112 GBd NRZ and PAM4. In order to keep the sensitivity penalty below 0.1 dB, the integrated crosstalk should not exceed -23.5 dB for NRZ and -31.0 dB for PAM4.

We define two groups of channels: Neighboring and non-neighboring channels. We assume equal crosstalk contributions from all 5 non-neighboring channels. Likewise, we assume equal crosstalk contributions from both neighboring channels. The sensitivity penalty as a function of crosstalk from neighboring and non-neighboring channels is illustrated in Fig. 5. From these contour plots, assuming a non-neighboring channel crosstalk of < -40 dB, we extract a neighboring channel crosstalk target of < -27.0 dB and < -38.4 dB for NRZ and PAM4, respectively, for a sensitivity penalty below 0.1 dB.

The crosstalk between neighboring channels is predominantly determined by the steepness of the filter. For a flattop filter this is often characterized by the 1 dB / 20 dB bandwidth ratio. E.g. the bandwidth ratio of a perfect rectangular filter (with no crosstalk) would be 1, while a typical bandwidth ratio for a flattop AWG in PLC is around 0.41 [26]. Assuming the minimum 1 dB bandwidth of 150 GHz from Fig. 3(a), the resulting 20 dB bandwidth of such AWG filter would be 341 GHz (±170.5 GHz). We can see that such a flattop filter cannot support < -27 dB neighboring channel crosstalk for an (ADOPTION) CPO with 200 GHz grid, however, such filter may be sufficient for systems with 400 GHz grid, as the extrapolated crosstalk at ±300 GHz is -44 dB. Therefore, a 400 GHz AWG grid was selected, as it combines low crosstalk with a wide flattop passband that provides adequate thermal margin for passive operation over data center temperature ranges and stable alignment with 112 GBd CPO transceivers without active wavelength control.

This article has been accepted for publication in Journal of Lightwave Technology. This is the author's version which has not been fully edited and
content may change prior to final publication. Citation information: DOI 10.1109/JLT.2026.3660127

IV. Silica-on-silicon platform

The cascaded AWG of this work has been fabricated on a silica-on-silicon platform. The refractive index contrast between SiO_2 waveguide core and SiO_2 waveguide cladding is approximately 0.019. The simulated fundamental TE mode at a wavelength of 1300 nm of a waveguide with 4 µm width and 6 µm height is depicted in Fig. 6. The mode field diameters of the mode are 4.75 µm × 6.27 µm. The manufacturing process flow of the AWG is illustrated in Fig. 7. A crystalline silicon substrate (1) gets thermally oxidized (2). The resulting thermal oxide layer has a thickness of 16 µm. A 6 µm-thick core Germanium-doped SiO_2 layer is then deposited (3) on top of the thermal oxide via Flame Hydrolysis Deposition (FHD). The core oxide is then patterned through lithography (4) and dry etching (5). After etching, a 22 µm-thick cladding oxide layer is deposited via FHD (6). For improving the crosstalk between neighboring channels, as will be discussed in section V, an additional lithography (7) and SiO_2 etching (8) step is performed, followed by a local deposition of black paint (9).

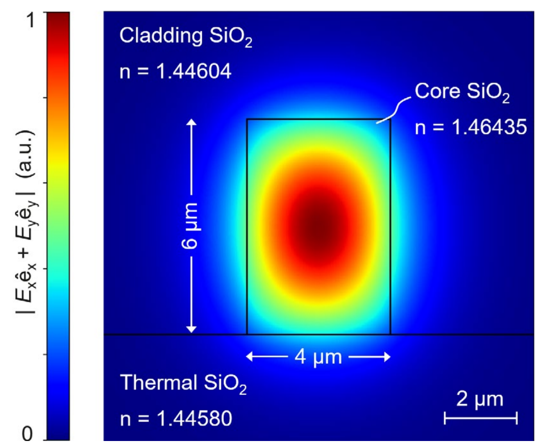

Fig. 6. Simulated mode profile of the fundamental TE mode of a 4 µm wide waveguide core.

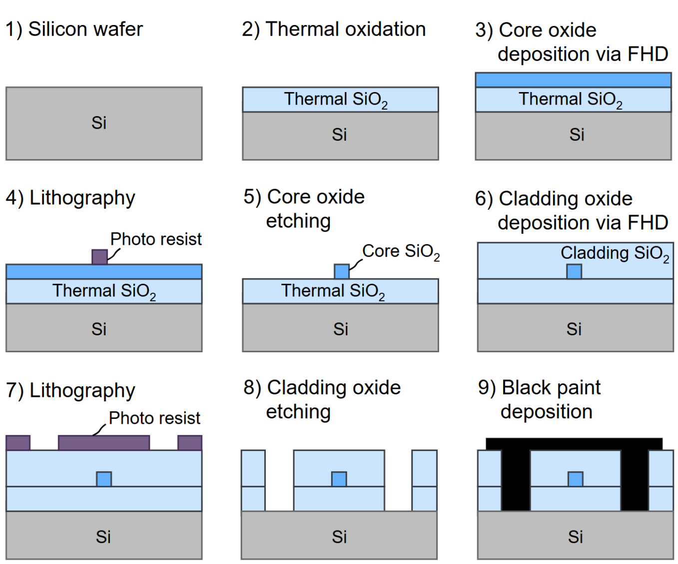

Fig. 7. Manufacturing process flow.

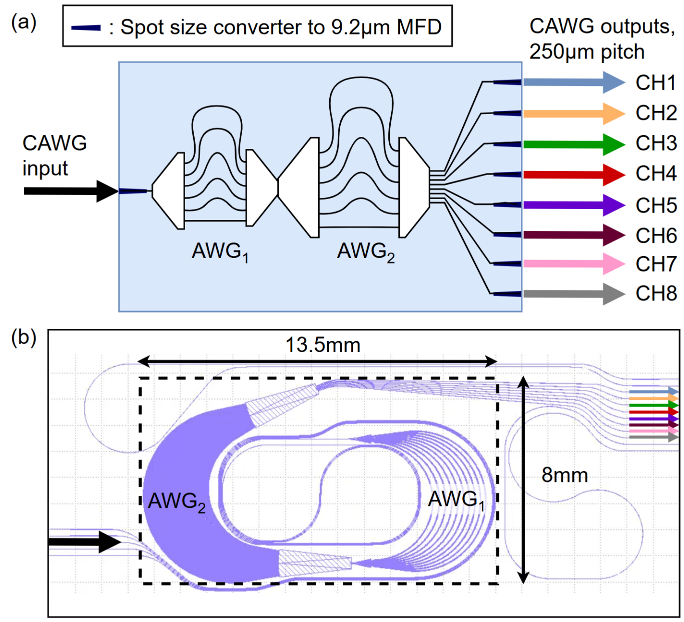

Fig. 8. Cascaded AWG layout. (a) Schematic. (b) Layout.

TABLE IV
CAWG design parameters.

Design parameter	AWG₁	AWG₂
Number of arrayed waveguides	10	165
Width of arrayed waveguides	6 µm	4 µm
Path length difference	505.195 µm	35.689 µm
Focal length	664.814 µm	3384.670 µm
Spacing of output waveguides	-	29.6 µm
Width of input/output WGs	4 µm	4 µm
Minimum bend radius	2250 µm	2250 µm
Diffraction number	566	40
Free spectral range	0.400 THz	5.659 THz

V. Cascaded AWG design

The CAWG consists of two directly joint AWGs. The individual AWGs have been designed following the design approach described by Dragone [36] where the first 1×1 AWG has a free spectral range of 400 GHz and the second 1×8 AWG has a channel spacing of 400 GHz. The 1×1 stage pre-shapes the spectrum by creating a spot that travels the Brillouin zone of AWG_1 for the duration of one order. The 1×8 stage has eight spots moving at the same location, one for each output, each being synchronized for the duration of exactly one order of AWG_1. Because both stages are spectrally synchronized, their fields combine coherently to produce a flatter, broader, and lower-loss response than a single AWG can achieve.

The layout of the cascaded AWG is depicted in Fig. 8. Spot size converters are used to convert the mode field diameter to ~9 µm for efficient coupling to standard single mode fibers. Optical loopbacks are included in the PIC layout for simplifying the optical alignment procedure of the fiber array units.

This article has been accepted for publication in Journal of Lightwave Technology. This is the author's version which has not been fully edited and
content may change prior to final publication. Citation information: DOI 10.1109/JLT.2026.3660127

The key design parameters of AWG_1 and AWG_2, e.g. the number of arrayed waveguides, their dimensions and spacing, the path length difference between adjacent waveguides, the minimum radius, and the focal length, are summarized in TABLE IV. The eight output waveguides of the second AWG are located on a circle with diameter equal to its focal length (Rowland mounting). All input and output waveguides have a width of 4 µm.

For illustration of the superior bandwidth and insertion loss, we compare the measured passband of the AWG cascade with the measured passband of a regular flattop AWG that uses a non-adiabatic taper on the input side, see Fig. 9(a). The AWG cascade has significantly lower loss and a much squarer passband than the single flattop AWG counterpart [29]. Due to the adjacent order diffraction modes from the first AWG entering the second AWG one will observe detrimental sidelobes in the passband approximately one channel away from the central wavelength of each channel. These sidelobes can be eliminated by creating an iris, as proposed by Maru et al. [37], i.e. by etching a slot which is subsequently filled with black paint, at the location where the first and second AWG meet. A microscope image of this section with etched iris, prior and after deposition of black paint is depicted in Fig. 10. A comparison of the achieved crosstalk with and without applied iris is shown in Fig. 9(b). By reducing the aperture of the iris one can further improve the isolation as the stopband is squeezed while the passband is maintained.

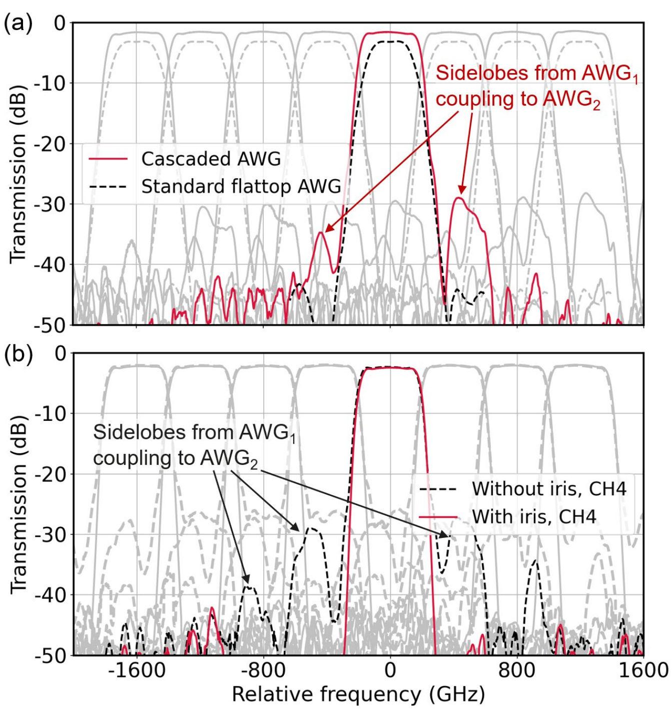

Fig. 9. (a) Measured transmission spectra of a cascaded AWG vs. a standard flattop AWG with non-adiabatic taper on the input side. (b) Measured transmission spectra of a cascaded AWG without and with iris. The iris successfully suppresses the sidelobes, thus improving the device crosstalk.

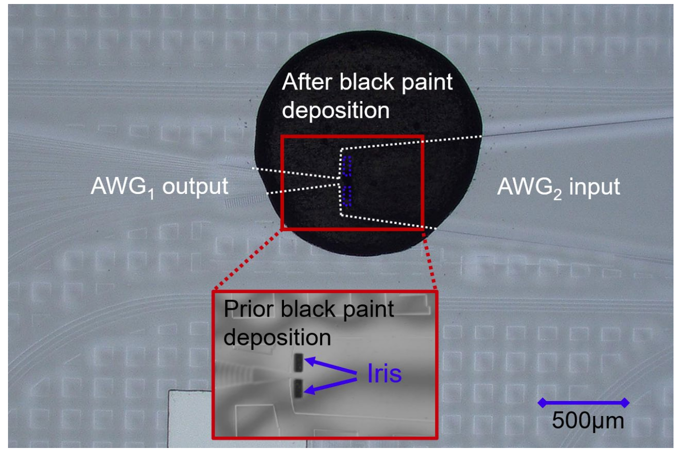

Fig. 10. To reduce crosstalk between channels, an iris is created at the location where the first and second AWG meet (white dashed lines). The iris is realized by etching a slot which is subsequently filled with black paint.

The CAWG samples have been fabricated in the cleanroom facility of Broadex Technologies UK, following the manufacturing process flow as depicted in Fig. 7. Individual dies are separated via dicing. The optical facets were 8° angle-polished after dicing. A total of 20 devices have been fabricated and tested. A photograph of a fabricated sample is depicted in Fig. 11(a). The samples were tested prior to and after pigtailing the chips with fiber array units (FAU). FAU-to-chip coupling losses are 0.4 dB per interface. A picture of a pigtailed CAWG is depicted Fig. 11(b). The AWG is mounted on a Kovar substrate for good thermal conductivity during thermal testing.

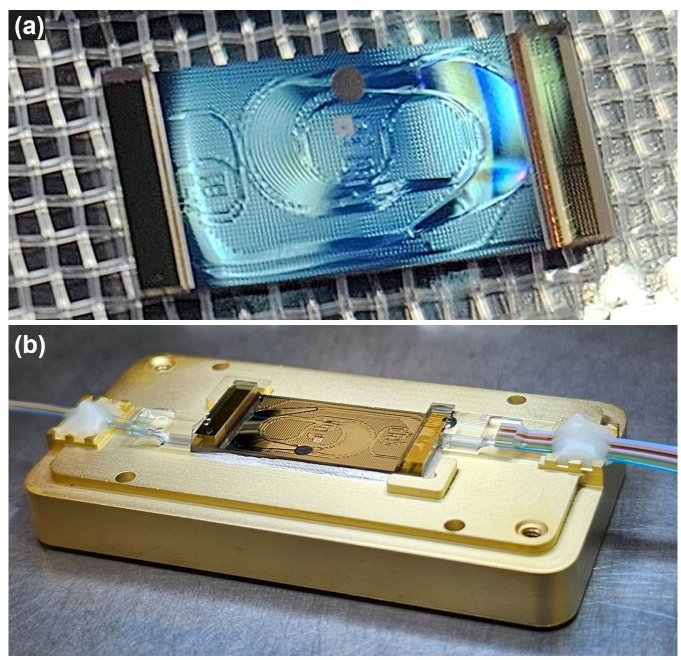

Fig. 11. Photograph of (a) a fabricated CAWG PLC and (b) of a packaged device. The PIC is pigtailed with a 5-channel FAU at the input and a 12-channel FAU at the output. 4 fibers per FAU are exclusively used for alignment loopback. The PIC is mounted on a Kovar substrate for good thermal conductivity during thermal testing.

VI. Test results

The fabricated samples have been tested prior and after pigtailing. Die testing was performed with a tunable laser source, a polarization controller, an SMF FAU at the CAWG input, an MMF FAU at the CAWG outputs, and a power meter array terminating the outputs. The Mueller Matrix analysis [38] is used for evaluating the polarization dependent loss of the CAWG channels. The pigtailed samples are characterized using an O-band broadband source and an optical spectrum analyzer. Fig. 12 depicts exemplary transmission spectra of a pigtailed AWG. The gray dotted lines indicate the targeted center frequency of the pass-bands. The gray bands indicate the targeted 200 GHz input frequency spans for the input signals. Our crosstalk values refer to these gray 200 GHz spans, assuming a signal bandwidth of ~125 GHz. The average crosstalk between neighboring channels is below -45 dB.

When measuring the insertion loss (IL) of the channels, we must consider the bandwidth of the expected input signals of ~125 GHz. Therefore, we perform a conversion of the resolution bandwidth (RBW) of the measured spectra from 3.5 GHz to 125 GHz as depicted in Fig. 13. The measured IL varies from channel to channel between 2.6 dB to 2.8 dB.

We characterize IL, PDL, frequency offset, grid, 1 dB bandwidth and crosstalk of all 8 channels on 20 samples before pigtailing and partially after pigtailing. The IL and PDL distributions of the devices are depicted in Fig. 14. Violin plots are visualizing the channel-to-channel variation. Prior pigtailing, the best device had an IL of 2.3 dB. After pigtailing, the best device has a mean IL of 2.7 dB, while the average IL of the pigtailed samples is 3.2 dB. The typical PDL is below 0.5 dB; 0.2 dB on average.

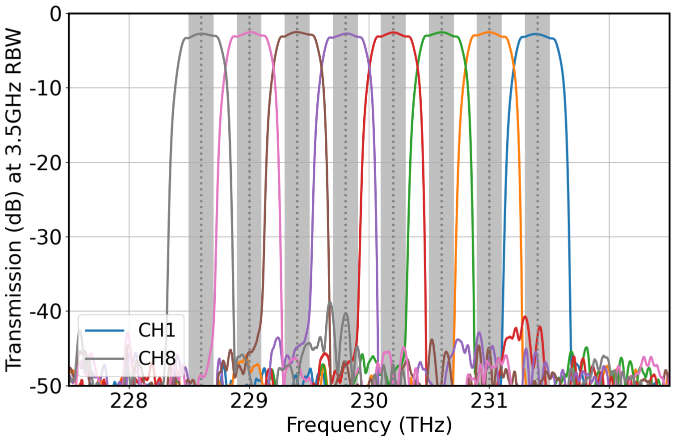

Fig. 12. Measured transmission spectra of the 8 AWG outputs. The gray dashed line and the gray areas indicate the targeted passbands. RBW set to 3.5 GHz. The background crosstalk level is around -45 dB.

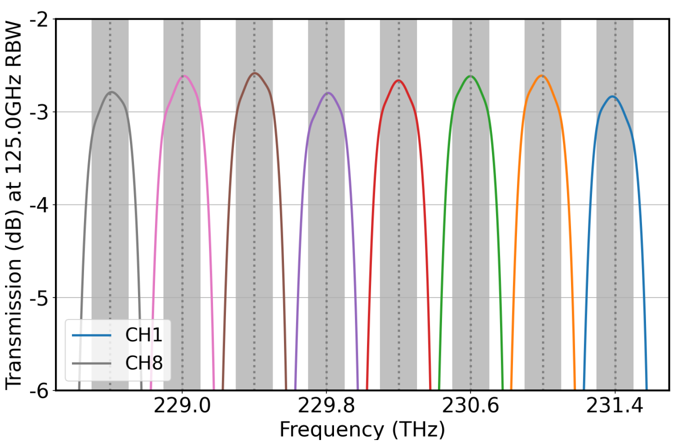

Fig. 13. Measured spectra at coarse (125 GHz) resolution bandwidth to illustrate the insertion loss for a 112 GBd signal. The measured insertion loss varies from channel to channel between -2.6dB and -2.8dB.

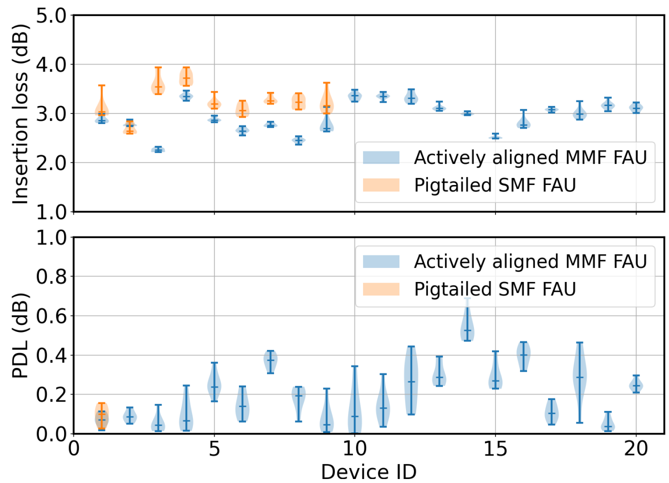

Fig. 14. Measured insertion loss and polarization dependent loss of 20 devices before and after pigtailing. The violin plots depict the distribution within each set of 8 channels.

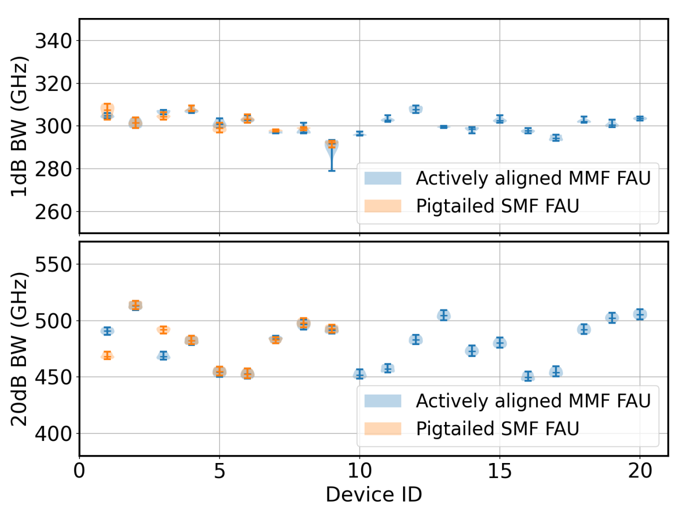

Fig. 15. Measured 1 dB bandwidth and 20 dB bandwidth of 20 devices before and after pigtailing. The violin plots depict the distribution within each set of 8 channels.

This article has been accepted for publication in Journal of Lightwave Technology. This is the author's version which has not been fully edited and content may change prior to final publication. Citation information: DOI 10.1109/JLT.2026.3660127

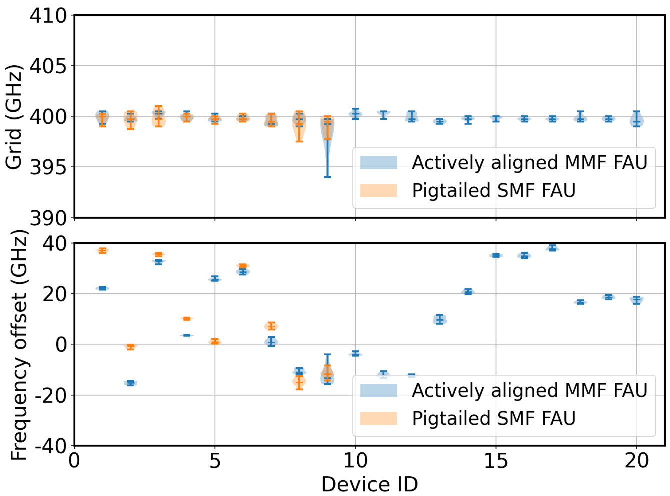

Fig. 16. Measured channel grid and frequency offset from target of 20 devices before and after pigtailing. The violin plots depict the distribution within each set of 8 channels.

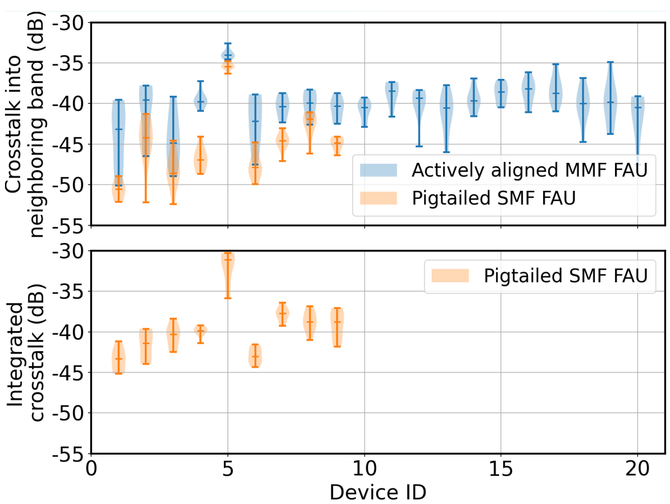

Fig. 17. Measured crosstalk to neighboring channels and integrated crosstalk of 7 neighboring channels. The violin plots depict the distribution within each set of 8 channels.

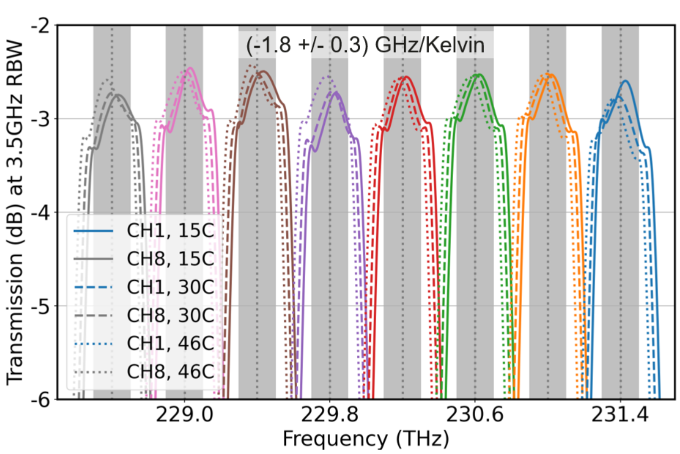

Fig. 18. AWG transmission spectra measured at 15°C, 30°C and 46°C. RBW set to 3.5 GHz.

Fig. 15 depicts the distributions of the bandwidth. The 1 dB bandwidth is (300.8 ± 4.4) GHz and 20 dB bandwidth is (479.5 ± 20.0) GHz. The resulting 1 dB to 20 dB bandwidth ratio is (0.63 ± 0.03). The distributions of grid and passband center frequency offset from the target are depicted in Fig. 16. The measured grid is (399.8 ± 0.4) GHz. Observed frequency offsets remain below 40 GHz at room temperature.

The measured crosstalk is shown in Fig. 17. The crosstalk into neighboring bands is on average below -40.2 dB prior pigtailing. During die testing the measured crosstalk level was limited by stray light captured by the large aperture of the multi-mode FAU used to probe the output waveguides to simplify coupling. After pigtailing the output with a single mode fiber array unit, less stray light is coupling into the output fibers and the measured average crosstalk improves further to -45.1 dB. The measured integrated crosstalk is (-39.6 ± 3.2) dB.

Finally, we characterize the temperature drift of the CAWG passband center frequencies by mounting a pigtailed sample onto a TEC. The CAWG spectra are measured at 15 °C, 30 °C, and at 46 °C, see Fig. 18. The measured thermal drift of (-1.8 ± 0.3) GHz/K is in line with the original estimation of -1.8 GHz/K based on the thermo-optic coefficient of glass [18] and including the contribution from thermal expansion of the relative path length differences.

A summary of our experimental results and a comparison with the device specifications from TABLE I is depicted in TABLE V. It can be seen that all targets are met for both NRZ and PAM4 operation, proving that the device performance is well suitable for expanding the radix of 400 GHz WDM transceivers for high-switch radix data center networks. Furthermore, the consistent results from 20 devices proves that the design is well manufacturable.

The performance of our flattop CAWG design is compared to prior art flattop designs in PLC, silicon and Si_3N_4. A high-level comparison of the insertion loss and flattop shape of the reviewed filters is illustrated in TABLE VI. We find that the CAWG passband outperforms previously reported flattop AWGs in PLC [26] both in terms of insertion loss and in terms of its rectangular shape. Resonant integrated photonic filters based on ring cascades [39] or Bragg gratings [40] can also feature comparable 1 dB to 20 dB bandwidth ratios (~0.6), however, their functionality is limited to a single polarization and channel. Cascading such single channel filters for WDM and applying polarization diversity can overcome this limitation, however, at the cost of increasing the DEMUX insertion loss.

TABLE V

COMPARISON OF ACHIEVED PERFORMANCE AGAINST TARGET SPECIFICATION (TABLE I), INCLUDING FIBER COUPLING LOSSES.

Parameter	**Measured (best / average)**	**Target (NRZ / PAM4)**
Insertion loss	2.7 dB / 3.2 dB	< 3.5 dB
1dB bandwidth	307.8 GHz / 300.8 GHz	> 220 GHz
Grid	400 GHz / 399.8 GHz	400 GHz
Crosstalk from neighboring channels	-50.7 dB / -45.1 dB	< -27.0 dB / < -38.4 dB
Integrated crosstalk	< -43.4 dB / < -39.6 dB	< -23.5 dB / < -31.0 dB

TABLE VI

COMPARISON OF ACHIEVED DEVICE PERFORMANCE WITH PREVIOUSLY PUBLISHED FLATTOP DEMUX DEVICES, EXCLUDING FIBER COUPLING LOSSES (2× 0.4 DB).

Reference	**Approach**	**1dB-to-20dB bandwidth ratio**	**Channel insertion loss (dB)**
This work	Cascaded PLC AWG	0.63 ± 0.03 (0.67 best)	2.4 ± 0.3 (1.9 best)
[26]	PLC MZI-AWG	0.54	3.2
[26]	Single PLC AWG (Flattop)	0.41	4.7
[29]	Cascaded SiN AWG	Not reported	4.0
[39]	5 coupled SiPh ring resonators (single pol. + active tuning)	~0.6	2.2 (single channel)

VII. CONCLUSION

We experimentally demonstrated a flattop PLC-based O-band 8-channel cascaded AWG design with 400 GHz channel spacing, simultaneously reaching a 1 dB bandwidth of 300 GHz and a crosstalk below -40 dB. The device has a steep filter response with 1 dB to 20 dB bandwidth ratio of 0.67. The measured fiber-to-fiber loss is as low as 2.7 dB and the PDL is below 0.2 dB. The combination of low IL, high bandwidth, low crosstalk, and reproducible manufacturability make the device particularly attractive for WDM-based data center and AI networks architectures that benefit from a large network switch radix.

REFERENCES

[1] P. Maniotis, L. Schares, B. G. Lee, M. A. Taubenblatt, and D. M. Kuchta, "Toward lower-diameter large-scale HPC and data center networks with co-packaged optics," *J. Opt. Commun. Netw.*, vol. 13, no. 1, p. A67, Jan. 2021, doi: 10.1364/JOCN.402676.

[2] Y. Fan, M. Luo, C. Liu, and S. Zhang, "Thermal solution study of 51.2T Near-packaged optics switch," in *2023 22nd IEEE Intersociety Conference on Thermal and Thermomechanical Phenomena in Electronic Systems (ITherm)*, Orlando, FL, USA: IEEE, May 2023, pp. 1–8. doi: 10.1109/ITherm55368.2023.10177553.

[3] "Broadcom Announces Tomahawk® 6 – Davisson, the Industry's First 102.4-Tbps Ethernet Switch with Co-Packaged Optics." [Online]. Available: https://www.broadcom.com/company/news/product-releases/63626

[4] D. Ye, C. S. Geyik, Z. Qian, and K. Aygün, "Package Technology Enabling for 224 Gbps Electrical Signaling," in *2023 IEEE 32nd Conference on Electrical Performance of Electronic Packaging and Systems (EPEPS)*, Oct. 2023, pp. 1–3. doi: 10.1109/EPEPS58208.2023.10314950.

[5] S. Kannan *et al.*, "High Density Integration of Silicon Photonic Chiplets for 51.2T Co-packaged Optics," in *2024 IEEE 74th Electronic Components and Technology Conference (ECTC)*, May 2024, pp. 81–84. doi: 10.1109/ECTC51529.2024.00022.

[6] P. Ossieur *et al.*, "Integrated Photonics and Electronics for Optical Transceivers Supporting AI/ML Applications," *IEEE J. Sel. Top. Quantum Electron.*, vol. 31, no. 3: AI/ML Integrated Opto-electronics, pp. 1–16, May 2025, doi: 10.1109/JSTQE.2025.3539379.

[7] Y. Wang *et al.*, "Co-Designed Silicon Photonics Chip I/O for Energy-Efficient Petascale Connectivity," *IEEE Trans. Compon. Packag. Manuf. Technol.*, vol. 15, no. 8, pp. 1581–1591, Aug. 2025, doi: 10.1109/TCPMT.2024.3492189.

[8] "PANDA PM Fibers for Co-packaged Optics." [Online]. Available: https://www.corning.com/catalog/coc/documents/product-family-specifications/OEM-142-AEN.pdf

[9] L. Brusberg *et al.*, "Glass Interposer for High-Density Photonic Packaging," in *Optical Fiber Communication Conference (OFC) 2022*, San Diego, California: Optica Publishing Group, 2022, p. Tu3A.3. doi: 10.1364/OFC.2022.Tu3A.3.

[10] C. S. Levy *et al.*, "8-$\lambdab $ $\times$ 50 Gbps/$\lambdab$ Heterogeneously Integrated Si-Ph DWDM Transmitter," *IEEE J. Solid-State Circuits*, pp. 1–12, 2024, doi: 10.1109/JSSC.2023.3344072.

[11] Q. Deng *et al.*, "Ultra-compact silicon rings with high thermal tuning efficiency demonstrated as an 8×400 GHz WDM filter," in *2025 Optical Fiber Communications Conference and Exhibition (OFC)*, Mar. 2025, pp. 1–3.

[12] A. Bayoumi *et al.*, "Enhanced Operation Range of Silicon MZI Filters Using a Broadband Bent Directional Coupler," *IEEE Photonics Technol. Lett.*, vol. 37, no. 9, pp. 501–504, May 2025, doi: 10.1109/LPT.2025.3553059.

[13] M. R. S. Katebzadeh, P. Costa, and B. Grot, "Evaluation of an InfiniBand Switch: Choose Latency or Bandwidth, but Not Both," in *2020 IEEE International Symposium on Performance Analysis of Systems and Software (ISPASS)*, Boston, MA, USA: IEEE, Aug. 2020, pp. 180–191. doi: 10.1109/ISPASS48437.2020.00033.

[14] S. Pathak, P. Dumon, D. Van Thourhout, and W. Bogaerts, "Comparison of AWGs and Echelle Gratings for Wavelength Division Multiplexing on Silicon-on-Insulator," *IEEE Photonics J.*, vol. 6, no. 5, pp. 1–9, Oct. 2014, doi: 10.1109/JPHOT.2014.2361658.

[15] Q. Wang and S. He, "Optimal design of a flat-top interleaver based on cascaded M–Z interferometers by using a genetic algorithm," *Opt. Commun.*, vol. 224, no. 4–6, pp. 229–236, Sept. 2003, doi: 10.1016/j.optcom.2003.07.016.

[16] C. Bluemm *et al.*, "Hardware-Efficient Duobinary Neural Network Equalizers for 800 Gb/s IM/DD PAM4 Transmission Over 10 km SSMF," *J. Light. Technol.*, vol. 41, no. 12, pp. 3783–3790, June 2023, doi: 10.1109/JLT.2023.3268579.

[17] C. R. Doerr and K. Okamoto, "Advances in Silica Planar Lightwave Circuits," *J. Light. Technol.*, vol. 24, no. 12, pp. 4763–4789, 2006, doi: 10.1109/JLT.2006.885255.

[18] G. Rego, "Temperature Dependence of the Thermo-Optic Coefficient of SiO2 Glass," *Sensors*, vol. 23, no. 13, 2023, doi: 10.3390/s23136023.

[19] F. G. Della Corte, G. Cocorullo, M. Iodice, and I. Rendina, "Temperature dependence of the thermo-optic coefficient of InP, GaAs, and SiC from room temperature to 600 K at the wavelength of 1.5 μm," *Appl. Phys. Lett.*, vol. 77, no. 11, pp. 1614–1616, Sept. 2000, doi: 10.1063/1.1308529.

[20] B. J. Frey, D. B. Leviton, and T. J. Madison, "Temperature-dependent refractive index of silicon and germanium," in *Optomechanical Technologies for Astronomy*, E. Atad-Ettedgui, J. Antebi, and D. Lemke, Eds., SPIE, 2006, p. 62732J. doi: 10.1117/12.672850.

[21] N. G. Pruiti, C. Klitis, C. Gough, S. May, and M. Sorel, "Thermo-optic coefficient of PECVD silicon-rich silicon nitride," *Opt Lett*, vol. 45, no. 22, pp. 6242–6245, Nov. 2020, doi: 10.1364/OL.403357.

[22] S.-H. Jeong *et al.*, "Polarization Diversified 16λ Demultiplexer Based on Silicon Wire Delayed Interferometers and Arrayed Waveguide Gratings," *J. Light. Technol.*, vol. 38, no. 9, pp. 2680–2687, May 2020, doi: 10.1109/JLT.2020.2969240.

[23] S. Guerber *et al.*, "Polarization independent and temperature tolerant AWG based on a silicon nitride platform," *Opt. Lett.*, vol. 45, no. 23, p. 6559, Dec. 2020, doi: 10.1364/OL.411332.

[24] Y. Wang *et al.*, "Ultrawide-band Low Polarization Sensitivity 3-µm SOI Arrayed Waveguide Gratings," *J. Light. Technol.*, vol. 40, no. 11, pp. 3432–3441, June 2022, doi: 10.1109/JLT.2022.3167829.

[25] Q. Han, J. St-Yves, Y. Chen, M. Ménard, and W. Shi, "Polarization-insensitive silicon nitride arrayed waveguide grating," *Opt. Lett.*, vol. 44, no. 16, p. 3976, Aug. 2019, doi: 10.1364/OL.44.003976.

[26] H. Bulthuis, *Low loss CAWG design for Super-PON systems*, July 17, 2019. [Online]. Available: https://www.ieee802.org/3/cs/public/201907/20190717-Low_Loss_CAWG.pdf

[27] G. H. B. Thompson, R. Epworth, C. Rogers, S. Day, and S. Ojha, "An Original Low-Loss and Pass-Band Flattened Si0/sub 2/ on Si Planar Wavelength Demultiplexer," in *OFC '98. Optical Fiber Communication Conference and Exhibit. Technical Digest. Conference Edition. 1998 OSA Technical Digest Series Vol.2 (IEEE Cat. No.98CH36177)*, 1998, pp. 76–77. doi: 10.1109/OFC.1998.657220.

[28] C. Dragone, "Frequency routing device having a wide and substantially flat passband," U.S. Patent 5488680

[29] A. Van Wijk, C. R. Doerr, Z. Ali, M. Karabiyik, and B. I. Akca, "Compact ultrabroad-bandwidth cascaded arrayed waveguide gratings," *Opt. Express*, vol. 28, no. 10, p. 14618, May 2020, doi: 10.1364/OE.394783.

[30] "ADOPTION website." [Online]. Available: https://www.ucc.ie/en/adoption-project/

[31] M. Tan *et al.*, "Co-packaged optics (CPO): status, challenges, and solutions," *Front. Optoelectron.*, vol. 16, no. 1, p. 1, Mar. 2023, doi: 10.1007/s12200-022-00055-y.

[32] M. Rombouts, A. R. Zali, S. Andreou, L. Augustin, and N. Calabretta, "Densely Integrated Photonic 8×8 Broadcast & Select Space Switch for High-Capacity Interconnects," *J. Light. Technol.*, pp. 1–7, 2025, doi: 10.1109/JLT.2025.3608833.

[33] *CW-WDM MSA Technical Specifications*. [Online]. Available: https://cw-wdm.org/

[34] "Data Center Power Equipment Thermal Guidelines and Best Practices." ASHRAE, 2016.

[35] G. P. Agrawal, "Optical Receivers," in *Fiber-Optic Communication Systems*, John Wiley & Sons, Ltd, 2021, pp. 107–150. doi: https://doi.org/10.1002/9781119737391.ch4.

[36] C. Dragone, "Low-loss wavelength routers for WDM optical networks and high-capacity IP routers," *J. Light. Technol.*, vol. 23, no. 1, pp. 66–79, 2005, doi: 10.1109/JLT.2004.840050.

[37] K. Maru *et al.*, "Super-high-Δ athermal arrayed waveguide grating with resin-filled trenches in slab region," *Electron. Lett.*, vol. 40, pp. 374–375, Apr. 2004, doi: 10.1049/el:20040273.

[38] Keysight, "Polarization-Resolved Measurements using Mueller Matrix Analysis," Application Notes. [Online]. Available: https://www.keysight.com/us/en/assets/7018-01231/application-notes-archived/5989-1261.pdf

[39] F. Xia, M. Rooks, L. Sekaric, and Y. Vlasov, "Ultra-compact high order ring resonator filters using submicron silicon photonic wires for on-chip optical interconnects," *Opt Express*, vol. 15, no. 19, pp. 11934–11941, Sept. 2007, doi: 10.1364/OE.15.011934.

[40] R. Cheng and L. Chrostowski, "Spectral Design of Silicon Integrated Bragg Gratings: A Tutorial," *J. Light. Technol.*, vol. 39, no. 3, pp. 712–729, Feb. 2021, doi: 10.1109/JLT.2020.3035372.